Physical and non-physical energy in scattered wave source-receiver interferometry

Giovanni Angelo Meles[a)] and Andrew Curtis
School of GeoSciences, The University of Edinburgh, Grant Institute, The King's Buildings, Edinburgh EH9 3JW, United Kingdom

(Received 14 January 2013; revised 27 March 2013; accepted 9 April 2013)

Source-receiver interferometry allows Green's functions between sources and receivers to be estimated by means of convolution and cross-correlation of other wavefields. Source-receiver interferometry has been observed to work surprisingly well in practical applications when theoretical requirements (e.g., complete enclosing boundaries of other sources and receivers) are contravened: this paper contributes to explain why this may be true. Commonly used inter-receiver interferometry requires wavefields to be generated around specific stationary points in space which are controlled purely by medium heterogeneity and receiver locations. By contrast, application of source-receiver interferometry constructs at least kinematic information about physically scattered waves between a source and a receiver by cross-convolution of scattered waves propagating from and to any points on the boundary. This reduces the ambiguity in interpreting wavefields generated using source-receiver interferometry with only partial boundaries (as is standard in practical applications), as it allows spurious or non-physical energy in the constructed Green's function to be identified and ignored. Further, source-receiver interferometry (which includes a step of inter-receiver interferometry) turns all types of non-physical or spurious energy deriving from inter-receiver interferometry into what appears to be physical energy. This explains in part why source-receiver interferometry may perform relatively well compared to inter-receiver interferometry when constructing scattered wavefields. © *2013 Acoustical Society of America*. [http://dx.doi.org/10.1121/1.4802825]

PACS number(s): 43.30.Ft, 43.20.Bi, 43.20.Dk, 43.20.Fn [RKS] Pages: 3790–3801

I. INTRODUCTION

Seismic interferometry generally refers to any technique that performs the construction or synthesis of Green's functions between two locations by means of integration of the cross-correlation or convolution of other wavefields (Claerbout, 1968; Ricket and Claerbout, 1999; Campillo and Paul, 2003; Derode *et al*., 2003). Depending on the recording configuration, we distinguish between inter-receiver and inter-source interferometry. In inter-receiver interferometry one or both of a pair of receivers are surrounded by a closed boundary of sources [Fig. 1(A)]. The Green's function between the two receivers is then found by cross-correlating or convolving pairs of recorded wavefields generated by each of the sources and integrating the result around the boundary (Wapenaar 2003, 2004; van Manen *et al*., 2005, 2006; Wapenaar and Fokkema, 2006). In principle either background noise sources or impulsive sources can be used for correlational interferometry, leading to the additional distinction between passive or active source interferometry (Campillo and Paul, 2003; Wapenaar and Fokkema, 2006). Inter-source interferometry, which provides a method to compute the Green's function between two sources surrounded by a closed boundary of receivers [Fig. 1(B)], follows most directly by simply applying source-receiver reciprocity to inter-receiver interferometry theory (Hong and Menke, 2006; Curtis *et al*., 2009).

This paper mainly concerns a third type of interferometry called source-receiver interferometry (SRI); as the name suggests, this is the only form of interferometry which can generate Green's functions between a source and a receiver (Curtis and Halliday, 2010; Halliday and Curtis, 2010; Poliannikov, 2011; Poliannikov *et al*., 2012; Curtis *et al*., 2012). In the following we use the term "interferometry" (when used on its own) to refer to inter-receiver interferometry, but tutorials and overviews of the various forms of seismic interferometry are given in Curtis *et al*. (2006), Wapenaar *et al*. (2010a,c), and Galetti and Curtis (2012).

In recent years, the importance of seismic interferometry has emerged in many different fields of exploration geophysics. These include redatuming data sets to "virtual" (imagined) source or receiver locations (Bakulin and Calvert, 2004, 2006; Schuster and Zhou, 2006; Schuster, 2009), ground roll (surface waves) removal (Curtis *et al*., 2006; Dong *et al*., 2006; Halliday *et al*., 2007, 2010; Xue and Schuster, 2007), velocity analysis (King and Curtis, 2011, 2012; King *et al*., 2011), and imaging (Schuster and Ricket, 2000; Schuster *et al*., 2004; Thorbecke and Wapenaar, 2007; Vasconcelos *et al*., 2009, 2010; Halliday and Curtis, 2010; Sava and Vasconcelos, 2010; Ravasi and Curtis, 2013). Theoretically, interferometry requires a closed boundary of sources surrounding a pair of receivers, and the availability of both monopole and dipole sources on that boundary. Because both of these conditions are generally too demanding from a practical experimental point of view, implementations often involve dipole-to-monopole approximations, and evaluation of only part of the boundary integral. Many studies have discussed the potential advantages

a)Author to whom correspondence should be addressed. Electronic mail: gmeles@staffmail.ed.ac.uk

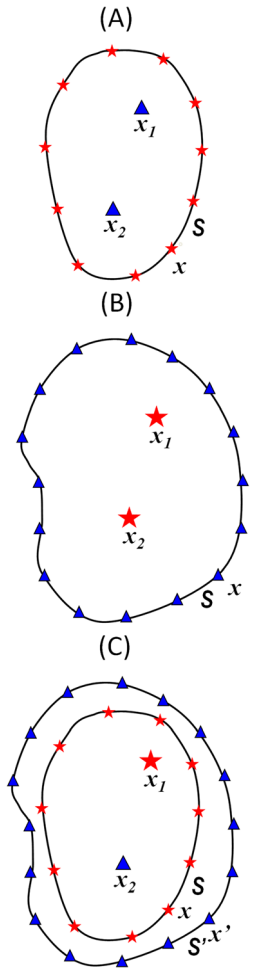

FIG. 1. (Color online) Geometrical configuration for inter-receiver (A), inter-source (B), and source-receiver (C) interferometry. Triangles and stars represent receivers and sources, respectively.

and limitations of partial or coarse source or receiver coverage (van Manen *et al.*, 2005; Snieder *et al.*, 2006; Mikesell *et al.*, 2009; King *et al.*, 2011; King and Curtis, 2011), while the phase errors associated with the monopole approximation have been shown to be reasonable under certain conditions (no back scattering, large radius boundary, and smoothness of the model where the derivatives would have been evaluated: Wapenaar and Fokkema, 2006). Partial fulfillment of the theoretical requirements of interferometry results in spurious or non-physical energy that contaminates Green's function estimates. The main contributions to the evaluation of the interferometric integrals come from neighborhoods of points where the interferometric integrand has stationary phase with respect to location on the boundary of integration (Snieder, 2004). Both physical and non-physical events are associated with such stationary points, and the lack of a complete boundary and consequent omission of such points can result in both the omission of physical energy, and the imperfect cancellation of non-physical energy.

The method of SRI was derived based on a combination of inter-source and inter-receiver interferometry (Curtis and Halliday, 2010; Halliday and Curtis, 2010). SRI allows the construction of Green's functions between a source and a receiver if Green's functions from and to closed boundaries of receivers and sources are available. SRI also allows recordings on a large variety of sensor types to be both spatially and temporally redatumed (Curtis *et al.*, 2012). Experimental evidence (Duguid *et al.*, 2011; Curtis *et al.*, 2012) and theoretical insights (Bharadwaj *et al.*, 2011; Poliannikov, 2011; King and Curtis, 2012) suggest that SRI may be more robust with respect to violations of the theoretical requirements of interferometry, particularly with respect to incompleteness of the supposedly closed boundaries, and to attenuation of energy within the medium. As a consequence, SRI has been shown to enhance existing methods of, for example, standard interferometric ground-roll removal (Duguid *et al.*, 2011).

In this paper we analyze scattered wave energy in the context of SRI, highlighting the differences from the standard inter-receiver case (which has already been studied extensively: Snieder *et al.*, 2008; Halliday and Curtis, 2009; Wapenaar *et al.*, 2010b). We show that intermediate, non-physical results of inter-receiver interferometry can be transformed into a proxy for physical events when convolved with other signals as prescribed by SRI. This may contribute to explaining the apparent robustness of the source-receiver method.

The first section below gives a brief introduction to the theory of inter-receiver and source-receiver interferometry. We then derive a new integral representation for the scattered wavefield which allows a new stationary phase analysis of the scattering problem. We use this to show that in general SRI can reproduce correct kinematic information about scattering, and even about dynamic waveforms, in situations where inter-receiver interferometry would fail. A discussion of synthetic tests quantitatively supports our arguments.

II. GREEN'S FUNCTION REPRESENTATIONS FOR INTER-RECEIVER AND SOURCE-RECEIVER INTERFEROMETRY

For acoustic media, frequency domain inter-receiver interferometry allows the sum of the Green's function and its complex conjugate (together known as the homogenous Green's function) between two receivers to be expressed as (Wapenaar and Fokkema, 2006)

$$G(x_2,x_1)+G^*(x_2,x_1) = \frac{-1}{j\omega\rho}\int_S \{G^*(x_2,x)n_i\partial_i G(x_1,x) - n_i\partial_i G^*(x_2,x)G(x_1,x)\}dS. \quad (1)$$

Here, j is the imaginary unit, ρ denotes the medium density, x_1 and x_2 indicate receiver positions, $G(x_2,x_1)$ represents the Green's function recorded at x_2 for an impulsive source at x_1, S stands for an arbitrary source boundary enclosing x_1 and x_2, and n_i and ∂_i represent the ith Cartesian component of the normal vector to S and of the gradient, respectively. Einstein summation over repeated indices is used here as in all of the following equations.

Equation (1) assumes constant density. Heterogeneous density distributions may be represented by simply moving $-1/j\omega\rho$ inside the integral. However, Eq. (1) is exact for an arbitrary velocity distribution even though there is no

explicit dependence on velocity—its effects are accounted for implicitly within the Green's functions.

Green's function representations are generally more easily derived in the frequency domain, while their interpretation is simpler in the time domain. Because the time domain equivalent of Eq. (1) involves cross-correlation of signals, we refer to Eq. (1) as correlation-based interferometry.

Combined application of inter-receiver and inter-source interferometry allows the homogeneous Green's function between a source and a receiver to be expressed as a double surface integral, a result known as source-receiver interferometry or SRI (Curtis and Halliday, 2010). In the acoustic case, for the geometry in Fig. 1(C), this result is

$$G(x_2,x_1)+G^*(x_2,x_1)=\frac{-1}{j\omega\rho}\int_S\left\{\left[\frac{-1}{j\omega\rho}\int_{S'}\{G^*(x',x_1)n_{i'}\partial_{i'}G(x',x)-n_{i'}\partial_{i'}G^*(x',x_1)G(x',x)\}dS'\right]n_i\partial_iG(x_2,x)\right.$$
$$\left.-\partial_in_i\left[\frac{-1}{j\omega\rho}\int_{S'}\{G^*(x',x_1)n_{i'}\partial_{i'}G(x',x)-n_{i'}\partial_{i'}G^*(x',x_1)G(x',x)\}dS'\right]G(x_2,x)\right\}dS. \quad (2)$$

Now x_1 and x_2 indicate source and receiver positions respectively, while S' stands for an arbitrary boundary of receivers at locations x' enclosing all of S, x_1 and x_2. Similar formulas exist for different geometries (e.g., involving a boundary of receivers enclosed by sources). The results presented in the next sections do not depend on a specific geometry, and for simplicity we will only refer to the configuration presented in Fig. 1(C).

Because for the geometry discussed above the term

$$\frac{-1}{j\omega\rho}\int_{S'}\{G^*(x',x_1)n_i\partial_iG(x',x)-n_i\partial_iG^*(x',x_1)G(x',x)\}dS' \quad (3)$$

is a real number [see Eq. (1)—the left hand side is always real], Eq. (2) is also equivalent to

$$G(x_2,x_1)+G^*(x_2,x_1)=\frac{-1}{j\omega\rho}\int_S\left\{\left[\frac{1}{j\omega\rho}\int_{S'}\{G(x',x_1)n_{i'}\partial_{i'}G^*(x',x)-n_{i'}\partial_{i'}G(x',x_1)G^*(x',x)\}dS'\right]n_i\partial_iG(x_2,x)\right.$$
$$\left.-\partial_in_i\left[\frac{1}{j\omega\rho}\int_{S'}\{G(x',x_1)n_{i'}\partial_{i'}G^*(x',x)-n_{i'}\partial_{i'}G(x',x_1)G^*(x',x)\}dS'\right]G(x_2,x)\right\}dS. \quad (4)$$

Approximate, more easily applicable formulas than Eqs. (1) and (4) can be written, respectively, for inter-receiver interferometry (Wapenaar and Fokkema, 2006)

$$G(x_2,x_1)+G^*(x_2,x_1)\approx\frac{2k}{\omega\rho}\int_S G(x_1,x)G^*(x_2,x)dS \quad (5)$$

and for source-receiver interferometry (Curtis and Halliday, 2010)

$$G(x_2,x_1)+G^*(x_2,x_1)\approx\frac{4k^2}{(\omega\rho)^2}\int_S\int_{S'}G(x',x_1)G^*(x',x)G(x_2,x)\,dS'\,dS. \quad (6)$$

Equations (5) and (6), which do not involve spatial derivative (dipole) sources, are valid in the high frequency limit and when waves travel approximately perpendicularly to boundaries.

Equations (1), (2), (4), (5), and (6) are often referred to as wavefield *representations* since they represent the wavefield Green's functions on the left hand side by using a set of other Green's function on the right.

A. Decomposition of interferometric integrals

Compact expressions of the inter-receiver representations in Eqs. (1) and (5) can be written by defining bilinear integral operators L and L^A (Wapenaar *et al.*, 2010b):

$$G(x_2,x_1)+G^*(x_2,x_1)=L[G_{x_1,x};\,G_{x_2,x}], \quad (7)$$

$$G(x_2,x_1)+G^*(x_2,x_1)\approx L^A[G_{x_1,x};\,G_{x_2,x}], \quad (8)$$

where the definitions of the bilinear operators are

$$L[G_{x_1,x};\,G_{x_2,x}]\equiv\frac{-1}{j\omega\rho}\int_S\{G^*(x_2,x)n_i\partial_iG(x_1,x)-n_i\partial_iG^*(x_2,x)G(x_1,x)\}dS, \quad (9)$$

$$L^A[G_{x_1,x};\,G_{x_2,x}]\equiv\frac{2k}{\omega\rho}\int_S\{G(x_1,x)G^*(x_2,x)\}dS \quad (10)$$

and where the superscript A on L^A stands for "approximate" and $G_{x_1,x}$ is a short-hand notation for $G(x_1,x)$.

A similar approach can be followed for the SRI case, whose representations in Eqs. (4) and (6) involve trilinear integral operators

$$G(x_2,x_1)+G^*(x_2,x_1)=\mathfrak{L}[G_{x',x_1};\,G_{x',x};\,G_{x_2,x}], \tag{11}$$

$$G(x_2,x_1)+G^*(x_2,x_1)\;\approx\;\mathfrak{L}^{\boldsymbol{A}}[G_{x',x_1};\,G_{x',x};\,G_{x_2,x}], \tag{12}$$

where the definition of the trilinear operators $\mathfrak{L}$ and $\mathfrak{L}^{\boldsymbol{A}}$ are

$$\begin{aligned}\mathfrak{L}[G_{x',x_1};\,G_{x',x};\,G_{x_2,x}]\equiv\frac{-1}{j\omega\rho}\int_S\Bigg\{&\left[\frac{1}{j\omega\rho}\int_{S'}\{G(x',x_1)n_{i'}\partial_{i'}G^*(x',x)-n_{i'}\partial_{i'}G(x',\,x_1)G^*(x',x)\}dS'\right]n_i\partial_iG(x_2,x)\\&-\partial_in_i\left[\frac{1}{j\omega\rho}\int_{S'}\{G(x',x_1)n_{i'}\partial_{i'}G^*(x',x)-n_{i'}\partial_{i'}G(x',\,x_1)G^*(x',x)\}dS'\right]G(x_2,x)\Bigg\}dS,\end{aligned} \tag{13}$$

$$\mathfrak{L}^{\boldsymbol{A}}[G_{x',x_1};\,G_{x',x};\,G_{x_2,x}]\equiv\frac{4k^2}{(\omega\rho)^2}\int_S\int_{S'}G(x',x_1)G^*(x',x)G(x_2,x)dS'\,dS. \tag{14}$$

We decompose each Green's functions into a known (e.g., modeled) background component G^0, and a scattered wave component G^S resulting from a perturbation in the medium's compressibility distribution, where G^S is defined by

$$G=G^0+G^S. \tag{15}$$

If we substitute Eq. (15) into Eqs. (7) and (8) we obtain

$$G(x_2,x_1)+G^*(x_2,x_1)=L[G^0{}_{x_1,x};\;G^0{}_{x_2,x}]+L[G^S{}_{x_1,x};\;G^0{}_{x_2,x}]+L[G^0{}_{x_1,x};\;G^S{}_{x_2,x}]+L[G^S{}_{x_1,x};\;G^S{}_{x_2,x}], \tag{16}$$

$$G(x_2,x_1)+G*(x_2,x_1)\approx L^A[G^0{}_{x_1,x};\;G^0{}_{x_2,x}]+L^A[G^S{}_{x_1,x};\;G^0{}_{x_2,x}]+L^A[G^0{}_{x_1,x};\;G^S{}_{x_2,x}]+L^A[G^S{}_{x_1,x};\;G^S{}_{x_2,x}]. \tag{17}$$

If instead we substitute Eq. (15) into Eqs. (11) and (12), due to the trilinearity of the integral operators $\mathfrak{L}$ and $\mathfrak{L}^{\boldsymbol{A}}$, we find

$$\begin{aligned}G(x_2,x_1)+G^*(x_2,x_1)=&\,\mathfrak{L}[G^0{}_{x',x_1};\,G^0{}_{x',x};\,G^0{}_{x_2,x}]+\mathfrak{L}[G^0{}_{x',x_1};\,G^S{}_{x',x};\,G^0{}_{x_2,x}]+\mathfrak{L}[G^0{}_{x',x_1};\,G^S{}_{x',x};\,G^S{}_{x_2,x}]\\&+\mathfrak{L}[G^0{}_{x',x_1};\,G^0{}_{x',x};\,G^S{}_{x_2,x}]+\mathfrak{L}[G^S{}_{x',x_1};\,G^0{}_{x',x};\,G^0{}_{x_2,x}]+\mathfrak{L}[G^S{}_{x',x_1};\,G^0{}_{x',x};\,G^S{}_{x_2,x}]\\&+\mathfrak{L}[G^S{}_{x',x_1};\,G^S{}_{x',x};\,G^0{}_{x_2,x}]+\mathfrak{L}[G^S{}_{x',x_1};\,G^S{}_{x',x};\,G^S{}_{x_2,x}],\end{aligned} \tag{18}$$

$$\begin{aligned}G(x_2,x_1)+G^*(x_2,x_1)\approx&\,\mathfrak{L}^{\boldsymbol{A}}[G^0{}_{x',x_1};\,G^0{}_{x',x};\,G^0{}_{x_2,x}]+\mathfrak{L}^{\boldsymbol{A}}[G^0{}_{x',x_1};\,G^S{}_{x',x};\,G^0{}_{x_2,x}]+\mathfrak{L}^{\boldsymbol{A}}[G^0{}_{x',x_1};\,G^S{}_{x',x};\,G^S{}_{x_2,x}]\\&+\mathfrak{L}^{\boldsymbol{A}}[G^0{}_{x',x_1};\,G^0{}_{x',x};\,G^S{}_{x_2,x}]+\mathfrak{L}^{\boldsymbol{A}}[G^S{}_{x',x_1};\,G^0{}_{x',x};\,G^0{}_{x_2,x}]+\mathfrak{L}^{\boldsymbol{A}}[G^S{}_{x',x_1};\,G^0{}_{x',x};\,G^S{}_{x_2,x}]\\&+\mathfrak{L}^{\boldsymbol{A}}[G^S{}_{x',x_1};\,G^S{}_{x',x};\,G^0{}_{x_2,x}]+\mathfrak{L}^{\boldsymbol{A}}[G^S{}_{x',x_1};\,G^S{}_{x',x};\,G^S{}_{x_2,x}].\end{aligned} \tag{19}$$

Thus, by using the representation provided by source–receiver rather than standard inter-receiver interferometry we decompose the homogeneous Green's function into the sum of eight rather than four terms. We will see below that this has some advantages.

As for the inter-receiver case, we note from Eq. (18) [using Eq. (15) if we do not perturb the medium, so $G^S=0$ and $G=G^0$] that we can retrieve the background Green's function as one element of the expanded expression

$$G^0(x_2,x_1)+G^{0*}(x_2,x_1)=\mathfrak{L}[G^0{}_{x',x_1};\,G^0{}_{x',x};\,G^0{}_{x_2,x}]. \tag{20}$$

Consequently, an expression for the scattered field involving only surface integrals is readily obtained by subtracting Eq. (20) from Eq. (18) as

$$\begin{aligned}&G^S(x_2,x_1)+G^{S*}(x_2,x_1)\\&\quad=\mathfrak{L}[G^0{}_{x',x_1};\,G^S{}_{x',x};\,G^0{}_{x_2,x}]+\mathfrak{L}[G^0{}_{x',x_1};\,G^S{}_{x',x};\;G^S{}_{x_2,x}]\\&\quad+\mathfrak{L}[G^0{}_{x',x_1};\,G^0{}_{x',x};\,G^S{}_{x_2,x}]+\mathfrak{L}[G^S{}_{x',x_1};\,G^0{}_{x',x};\,G^0{}_{x_2,x}]\\&\quad+\mathfrak{L}[G^S{}_{x',x_1};\,G^0{}_{x',x};\,G^S{}_{x_2,x}]+\mathfrak{L}[G^S{}_{x',x_1};\,G^S{}_{x',x};\,G^0{}_{x_2,x}]\\&\quad+\mathfrak{L}[G^S{}_{x',x_1};\,G^0{}_{x',x};\,G^S{}_{x_2,x}]\end{aligned} \tag{21}$$

and similarly for the approximate representation in Eq. (19) we have

$$G^S(x_2,x_1)+G^{S*}(x_2,x_1)\approx \mathfrak{L}^{\mathcal{A}}[G^0_{x',x_1};G^S_{x',x};G^0_{x_2,x}]+\mathfrak{L}^{\mathcal{A}}[G^0_{x',x_1};G^S_{x',x};G^S_{x_2,x}]+\mathfrak{L}^{\mathcal{A}}[G^0_{x',x_1};G^0_{x',x};G^S_{x_2,x}]$$
$$+\mathfrak{L}^{\mathcal{A}}[G^S_{x',x_1};G^0_{x',x};G^0_{x_2,x}]+\mathfrak{L}^{\mathcal{A}}[G^S_{x',x_1};G^0_{x',x};G^S_{x_2,x}]+\mathfrak{L}^{\mathcal{A}}[G^S_{x',x_1};G^S_{x',x};G^0_{x_2,x}]$$
$$+\mathfrak{L}^{\mathcal{A}}[G^S_{x',x_1};G^S_{x',x};G^S_{x_2,x}]. \quad (22)$$

These new representations contain only surface integrals. They may find applicability in imaging or inversion (Vasconcelos, 2011; Fleury and Vasconcelos, 2012) as an alternative to currently used formulations that involve both surface and volume integrals (Halliday and Curtis, 2010). This may be useful because volume integrals typically require too much computational power to be used in imaging representations and applications.

Both for the direct and scattered Green's function representations the main contributions to each integral come from points of the boundary where the integrand has a phase that is stationary with respect to location on the boundaries S or S' (Snieder, 2004). In the following we analyze the kinematics of the new representation in Eq. (18). We focus on the locations of stationary phase associated with each of the terms in the SRI Eq. (18) and compare them to those for the inter-receiver case in Eq. (16). In this paper we specifically examine these points for the case of a single scatterer in a homogeneous background medium. The results apply to the single scattering component of the wavefield for each and every scatterer in multiple-scatterer scenarios.

B. Stationary points in inter-receiver and source-receiver interferometry

One of the most important practical shortcomings associated with standard inter-receiver interferometry is the theoretical requirement of a full boundary of sources that encloses the receivers. In the case of incomplete boundaries (as in almost all practical problems) any distribution of stationary points in the integrand that occur at points outside of available portions of the boundary may result in amplitude or phase distortions of the physical features of wavefields constructed by interferometry, and imperfect cancellation of non-physical energy within those wavefields. We now analyze and compare the location and nature of stationary points for the single scatterer problem in the context of inter-receiver and source-receiver interferometry.

For the geometry depicted in Fig. 2(A), the distribution of stationary points of the four components resulting from the decomposition of the inter-receiver interferometric integrals [Eq. (16)] are summarized in Table I. The acausal and causal direct waves are reconstructed by sources distributed around the stationary points (a) and (b), the corresponding scattered waves by sources around (c) and (e), respectively. Non-physical events are constructed by sources around (d) and (f) which are stationary points of the integrands in $L[G^0_{x_1,x};G^S_{x_2,x}]$ and $L[G^S_{x_1,x};G^0_{x_2,x}]$. For the term only involving scattered waves, $L[G^S_{x_1,x};G^S_{x_2,x}]$, *any* point on the boundary is stationary (the integrand has constant phase) and contributes non-physical energy in the reconstructed Green's function. Figure 3 shows a corresponding analysis for $L[G^0_{x_1,x};G^S_{x_2,x}]$ and $L[G^S_{x_1,x};G^S_{x_2,x}]$.

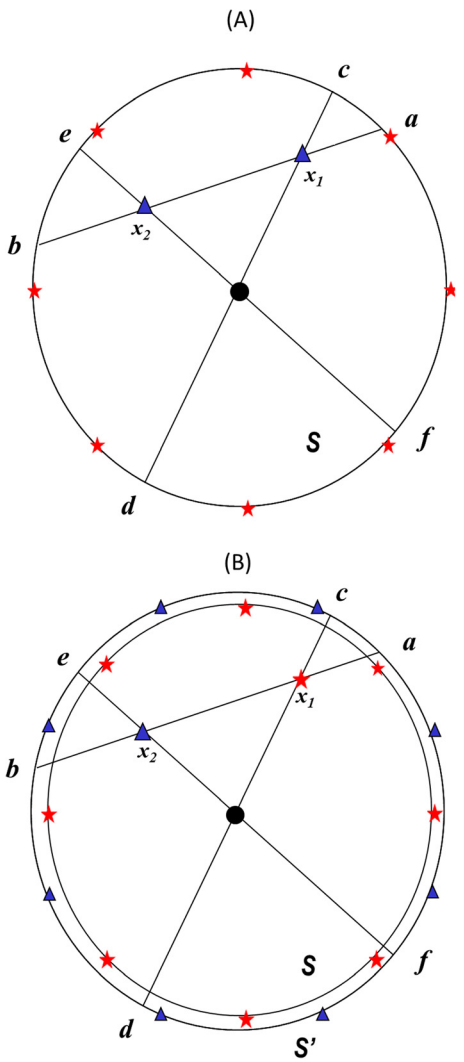

FIG. 2. (Color online) (A) Geometry for inter-receiver interferometry: a single point scatterer (filled circle) is embedded in a homogenous background medium. A boundary S of sources (stars) encloses receivers x_1 and x_2 (triangles). Locations of notable stationary points are labeled by letters (a–f). In addition to these discrete points, any source location is stationary for the term $L[G^S_{x_1,x};G^S_{x_2,x}]$. See Table I for a complete summary of these points. (B) Geometry for source-receiver interferometry (SRI): boundaries of sources and receivers enclose a single source and a single receiver at locations x_1 and x_2, respectively. Locations of notable stationary points are labeled by letters (a–f). In addition to these discrete points, a continuum of source/receiver location is stationary for the term $\mathfrak{L}[G^S_{x',x_1};G^0_{x',x};G^S_{x_2,x}]$ and $\mathfrak{L}[G^S_{x',x_1};G^S_{x',x};G^S_{x_2,x}]$ and provides the exact scattered wave travel times. See Table II for a complete summary of these points.

TABLE I. For the geometry of Fig. 2(A), summary of physical (bold) and non-physical (italic) stationary points of the single scattering problem. Underlined points indicate acausal physical events (those that occur at negative times). For the definition of the bilinear integral operator L, see Eq. (9).

Integral operators	Stationary points
$L[G^0_{x_1,x}; G^0_{x_2,x}]$	**x = a; x = b;**
$L[G^0_{x_1,x}; G^S_{x_2,x}]$	**x = c;** *x = d;*
$L[G^S_{x_1,x}; G^0_{x_2,x}]$	**x = e;** *x = f;*
$L[G^S_{x_1,x}; G^S_{x_2,x}]$	Any point;

The non-physical contributions in each of the above terms mutually cancel out if the entire boundary of sources is available, while physical events are constructed only if the appropriate stationary points are included in the available portion of the boundary. For the single scattering problem this means that to be able to extract information about the scattered wave from inter-receiver interferometry, availability of sources at locations (c) and (e) is mandatory. Moreover, energy constructed purely from scattered waves, namely, $L[G^S_{x_1,x}; G^S_{x_2,x}]$, is *never* representative of physical energy (Halliday and Curtis, 2009; Wapenaar *et al.*, 2010b).

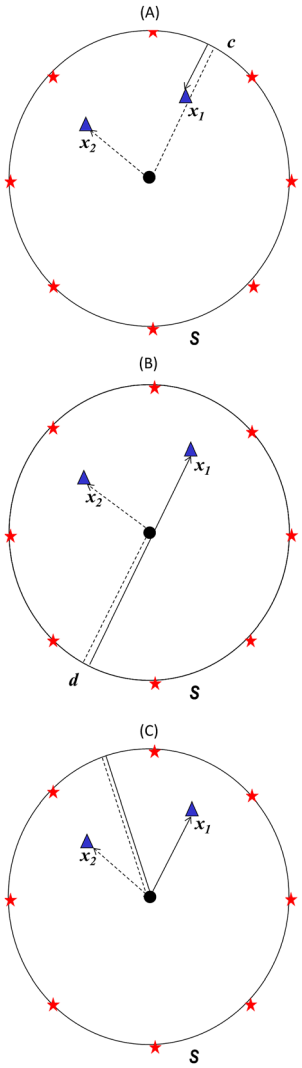

FIG. 3. (Color online) Construction of physical (A) or non-physical (B) scattered wave energy and corresponding stationary points of the integrand of $L[G^0_{x_1,x}; G^S_{x_2,x}]$. Solid and dashed lines indicate summation or subtraction of corresponding travel times (phases), respectively [in Eq. (1)]. (C) As for (A) and (B), but for $L[G^S_{x_1,x}; G^S_{x_2,x}]$ for which *any* point is stationary and provides non-physical energy. Key as in Fig. 2.

The situation is different for SRI. In Fig. 2(B) we consider the same single scattering problem as depicted in Fig. 2(A), but instead of a receiver a source is placed at x_1, and an additional boundary of receivers encloses all of the source boundary and both x_1 and x_2. For the eight components resulting from the decomposition of the interferometric integral, we have identified all corresponding stationary points, which are listed in Table II. The validity of all arguments discussed here is, however, not limited to the geometry depicted in Fig. 2(B) as the arguments neither depend on the exact position of the scatterer, nor on the shape of the boundaries. Note also that in inter-receiver interferometry, the main contributions to the reconstruction of Green's functions are associated with stationary points over the enclosing surface of the integrand (Schuster, 2009). The same holds for SRI, but since the corresponding integrand is a function of two boundary locations, we refer to such points as stationary point-pairs.

We illustrate this concept by analyzing the stationary point-pairs of the first term of Eq. (18), i.e., $\mathfrak{L}[G^0_{x',x_1}; G^0_{x',x}; G^0_{x_2,x}]$. Because the exact and approximate representations [Eqs. (4) and (6), respectively] share the same kinematics, for the identification of the stationary points of each of the terms of Eq. (18) we may also refer to the corresponding points of Eq. (19), which allows easier interpretation. Figure 4(A) shows the travel-time (equivalently, the phase) of the integrand of $\mathfrak{L}[G^0_{x',x_1}; G^0_{x',x}; G^0_{x_2,x}]$ (identical to that of $\mathfrak{L}^A[G^0_{x',x_1}; G^0_{x',x}; G^0_{x_2,x}]$, i.e., the phase of $G^0(x',x_1)G^{0*}(x',x)G^0(x_2,x)$) as a function of boundary source x and receiver x' positions. This diagram does not represent the amplitude of the integrand of $\mathfrak{L}[G^0_{x',x_1}; G^0_{x',x}; G^0_{x_2,x}]$ but rather is designed only to enable easy visualization of the stationary phase point-pairs.

There are four stationary point-pairs for the travel time of this function, indicated by circles and squares in Fig. 4(A). However, it turns out that the integrand is non-zero

TABLE II. For the geometry of Fig. 2(B), summary of kinematic physical (bold) and non-physical (italic) stationary point pairs of single scattering problem. Underlined points indicate acausal physical events (those that occur at negative times). For the definition of the trilinear operator $\mathfrak{L}$ see Eq. (13).

Integral operators	Stationary pairs
$\mathfrak{L}[G^0_{x',x_1}; G^0_{x',x}; G^0_{x_2,x}]$	**x = a, x′ = b; x = b, x′ = a;**
$\mathfrak{L}[G^0_{x',x_1}; G^0_{x',x}; G^S_{x_2,x}]$	**x = c, x′ = d;** *x = d, x′ = c;*
$\mathfrak{L}[G^0_{x',x_1}; G^S_{x',x}; G^S_{x_2,x}]$	*∀ x, x′ = c;* **∀ x, x′ = d;**
$\mathfrak{L}[G^0_{x',x_1}; G^S_{x',x}; G^0_{x_2,x}]$	**x = e, x′ = c;** *x = e, x′ = d;* **x = f, x′ = d;** *x = f, x′ = c;*
$\mathfrak{L}[G^S_{x',x_1}; G^0_{x',x}; G^0_{x_2,x}]$	**x = f, x′ = e;** *x = e, x′ = f;*
$\mathfrak{L}[G^S_{x',x_1}; G^S_{x',x}; G^0_{x_2,x}]$	**x = f, ∀x′;** *x = e, ∀ x′;*
$\mathfrak{L}[G^S_{x',x_1}; G^0_{x',x}; G^S_{x_2,x}]$	**Any pair connected by a straight line passing through the scatterer;**
$\mathfrak{L}[G^S_{x',x_1}; G^S_{x',x}; G^S_{x_2,x}]$	**Any pair;**

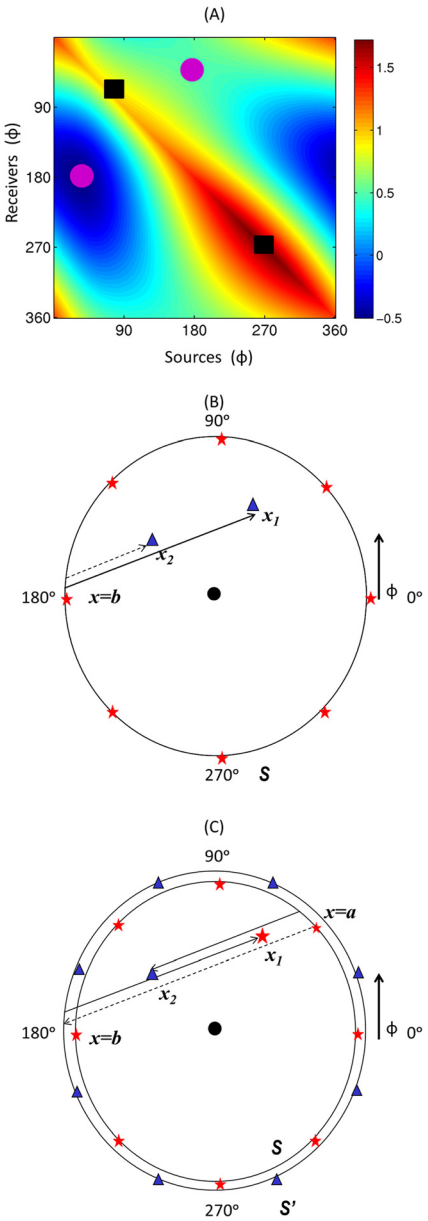

FIG. 4. (Color online) (A) Travel time corresponding to the integrand of $\mathfrak{L}[G^0_{x',x_1}; G^0_{x',x}; G^0_{x_2,x}]$ as a function of boundary source $x \in S$ and receiver $x' \in S'$ positions. Circles and squares indicate constructive and destructive stationary point pairs, respectively. (B) 3D representation of the surface in (a). Solid and dashed arrows indicate constructive and non-constructive point-pairs, respectively. (C) Construction of physical causal direct wave travel time in inter-receiver interferometry. Solid and dashed lines indicate summation or subtraction of respective travel times in Eq. (1). (D) Construction of physical direct wave travel times in source-receiver interferometry. Stationary point pairs involve the same points seen in the inter-receiver case in Fig. 2. Key as in Fig. 2.

only at the circles, while at the squares the terms of Eq. (4) interfere destructively: the first inter-source interferometry step intrinsic in source-receiver interferometry results in the causal Green's functions $G^0(x_1,x)$ being constructed from energy at and around the squares. During the successive inter-receiver step, these functions are convolved with other causal Green's functions [i.e., $G^0(x_2,x)$, see Eq. (4)]. However, for the geometry considered here, this operation does not produce any signal because the stationary points of its integrand involve zero amplitude signals as shown by Slob *et al.* (2007). This also negates the amplitude information in Eq. (6), which invokes a dipole approximation which is valid only when causal and acausal wavefields in inter-receiver or inter-source processes are combined (Wapenaar and Fokkema, 2006). To account for this, Curtis *et al.* (2012) introduced an improved monopole formula which separates and invokes only those combinations of causal and acausal fields in the inter-source and inter-receiver steps that produce the desired, physical results. However their equation does not benefit from the compactness and readability of the more commonly used Eq. (6). For the purposes of this paper we therefore use Eq. (6), discussing its limitations where appropriate.

The circle pairs correspond to point pairs (a,b) and (b,a) in Fig. 2(B), each of which also provide the direct wave information in the inter-receiver case (in the limit of collocated boundaries S and S'). There is therefore no substantial difference between the geometrical boundary requirements of the two methods so far as the direct wave is concerned. However, the correct travel times are constructed in quite different ways between the two methods. Figure 4(B) shows how the travel times are combined in inter-receiver interferometric integrals: the cross-correlation between $G^0(x_1,x)$ and $G^0(x_2,x)$ in Eq. (1), involves subtraction of the phase or travel time of $G^0(x_2,x)$ (dashed line) from the phase of $G^0(x_1,x)$ (solid line). The construction is more involved in source-receiver interferometry [Fig. 4(C)]: travel times along solid lines are associated with convolved traces and are summed (since phases are summed by convolution). The dashed line corresponds to the cross correlated trace, and its travel time is therefore subtracted from the cross convolution result. The result of these additions and subtractions prescribed by source-receiver interferometry [Eq. (6)] is a wave with the travel time of the direct wave between the source at x_1 and the receiver at x_2, since in both Figs. 4(B) and 4(C) the travel time along any portion of path spanned by one solid and one dashed line cancel.

We now focus on terms involving scattered wavefields. Table II gives a summary of all of the possible stationary configurations of all terms in Eqs. (18) and (19). For brevity, we only consider three representative combinations of direct and scattered wavefields in detail: $\mathfrak{L}[G^0_{x',x_1}; G^0_{x',x}; G^S_{x_2,x}]$, $\mathfrak{L}[G^S_{x',x_1}; G^0_{x',x}; G^S_{x_2,x}]$, and $\mathfrak{L}[G^S_{x',x_1}; G^S_{x',x}; G^S_{x_2,x}]$, that is, terms involving one, two, or three scattered wave components.

Figure 5(A) shows a stationary point pair of $\mathfrak{L}[G^0_{x',x_1}; G^0_{x',x}; G^S_{x_2,x}]$ that constructs correct scattered-wave traveltimes. Cancellation of common paths in the cross-correlation, together with summation of direct and scattered travel times by convolution, produces the correct scattered-wave kinematics for the stationary pair ($x=c$, $x'=d$). Also the pair ($x=d$, $x'=c$) is stationary, but this combination of points corresponds to a non-physical event as shown in Fig. 5(B). This pair was also noticeable for the inter-receiver case (see Table I).

The situation is different for $\mathfrak{L}[G^S_{x',x_1}; G^0_{x',x}; G^S_{x_2,x}]$: for this term, any point-pair connected by a straight line passing through the scatterer is stationary and provides the correct physical information about the causal scattered event travel time [Fig. 5(C)]. The true scattered wave travel time information is thus not restricted to two single stationary points

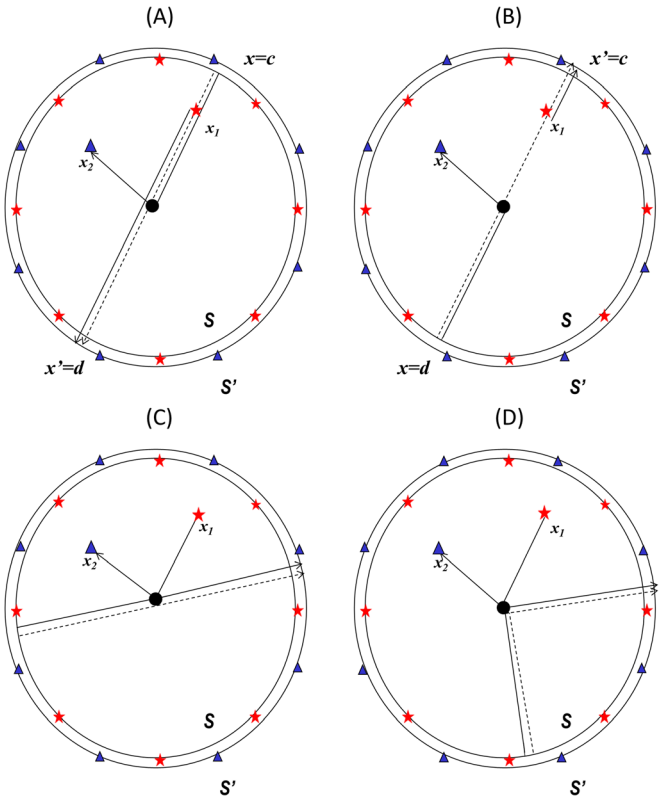

FIG. 5. (Color online) Stationary point pairs of the integrand of $\mathfrak{L}[G^0_{x',x_1}; G^0_{x',x}; G^S_{x_2,x}]$ for the construction of physical (A) or non-physical (B) scattered wave travel times. Solid and dashed lines indicate summation or subtraction of travel times, respectively. Stationary point pairs involve the same points as in the inter-receiver case. (C) as for (A) and (B), but for the integrand of $\mathfrak{L}[G^S_{x',x_1}; G^0_{x',x}; G^S_{x_2,x}]$: any point pair (x',x) connected by a straight line passing through the scatterer is stationary and provides physical scattered wave travel times. In contrast to the inter-receiver case, the stationary information is not now associated with only the four points (c,d,e,f) in Fig. 2. (D) As for (A) and (B), but for the integrand of $\mathfrak{L}[G^S_{x',x_1}; G^S_{x',x}; G^S_{x_2,x}]$: in this case *any* point pair (x',x) provides the physical scattered wave travel time. Key as in Fig. 2.

as it was for the inter-receiver case, but is now associated with a continuum of point pairs all around the boundary.

Finally for term $\mathfrak{L}[G^S_{x',x_1}; G^S_{x',x}; G^S_{x_2,x}]$, *any* point pair is stationary and provides the correct, causal scattered wave travel-time. Indeed, this result is not constrained to the current geometry but is valid for any single scatterer problem. Also, since all wavefield pairs connecting the boundary sources or receivers to the scatterer always involve causal and acausal components together [see Fig. 5(D)], the far field approximation does not suffer from the shortcoming of Eq. (6) mentioned earlier, as long as both boundaries enclose the scatterer. In the case that the scatterer lies outside of either boundary, $L[G^S_{x_1,x}; G^S_{x_2,x}]$ and therefore $\mathfrak{L}[G^S_{x',x_1}; G^S_{x',x}; G^S_{x_2,x}]$ do not contribute at all to the scattered wavefield (Fleury *et al.*, 2010), while $L^A[G^S_{x_1,x}; G^S_{x_2,x}]$ results in a non-zero amplitude, non-physical event due to the missing dipoles in the approximation. However, SRI provides the correct scattering kinematics through $\mathfrak{L}^A[G^S_{x',x_1}; G^S_{x',x}; G^S_{x_2,x}]$ also for this intermediate artifact. While for the other terms of Eq. (22) we only discussed kinematics, we now focus also on the amplitudes of the scattered waves associated with the term $\mathfrak{L}^A[G^S_{x',x_1}; G^S_{x',x}; G^S_{x_2,x}]$. To do so, we recall that for isotropic scatterers (Groeneboom and Snieder, 1995; Galetti and Curtis, 2013) the scattered field Ψ^S due to an incident field Ψ^0 can be expressed as

$$\Psi^S(x_a, x_b) = \Psi^0(x_D, x_a) A_D \bar{G}^0(x_b, x_D), \tag{23}$$

where x_a and x_b are any source-receiver positions, respectively, A_D represents the scattering potential, x_D is the position of the scatterer and $\bar{G}^0$ is the Green's function for the Helmholtz equation. Inserting Eq. (23) into each scattering term of $\mathfrak{L}^A[G^S_{x',x_1}; G^S_{x',x}; G^S_{x_2,x}]$ results in

$$\mathfrak{L}^A[G^S_{x',x_1}; G^S_{x',x}; G^S_{x_2,x}] = \lambda G^S(x_2, x_1), \tag{24}$$

where λ is a positive real number. For 2D problems it is easy to demonstrate that in the far field approximation λ does not depend on ω. In this scenario then $\mathfrak{L}^A[G^S_{x',x_1}; G^S_{x',x}; G^S_{x_2,x}]$ is proportional to the exact physical scattered field. In 3D, it can be shown that λ is a linear function of ω, thus allowing $\mathfrak{L}^A[G^S_{x',x_1}; G^S_{x',x}; G^S_{x_2,x}]$ to be transformed into a proxy for the physical scattered wave by simply dividing each frequency component by ω. This is also true for partial boundaries S and S'. This shows that in contrast to the inter-receiver case (Wapenaar *et al.*, 2010; Snieder and Fleury, 2010), in source-receiver interferometry a proxy for the true scattered waves can be constructed from purely scattered energy from the boundary, and *any* two boundary points will reproduce physical energy. This result is possibly the most important finding of our research, and therefore in the numerical experiment discussed in the next section we focus purely on scattered waves. We will show that using SRI in fact even only a single point pair can be sufficient to provide an excellent estimate of both the kinematics and the relative amplitude of scattered waves. This is important as it can dramatically reduce the severity of geometrical requirements on source or receiver boundaries (which remains necessary for other forms of interferometry). More precisely, while inter-receiver interferometry requires access to specific, *a priori* unknown, source locations to retrieve the scattered Green's function, in SRI any scattered-wave data provides the correct scattering kinematics.

III. NUMERICAL EXAMPLE: SINGLE SCATTERING PROBLEM

We support our analysis above with two-dimensional synthetic tests of interferometric waveform construction. We compute wavefields with a numerical implementation of the Foldy method (Foldy, 1945; Galetti and Curtis, 2013). This method is consistent with the optical theorem of scattering and hence correctly constrains the values of the scattering amplitudes such that energy is conserved (Groeneboom and Snieder, 1995). In our 2D example we use a background velocity of 1000 m/s, a unit density, and a single isotropic scatterer. Calculations are performed in the frequency domain, but for ease of interpretation we present results in the time domain. A Ricker wavelet with central frequency of 30 Hz is used to generate the wavefields. Because we are ultimately interested in realistic wavefields, in which dipole sources are seldom available, dipoles are not used in our synthetic

examples. This is equivalent to using Eqs. (6) and (17) instead of Eqs. (4) and (18). While providing different amplitudes, all of these representations retain the same phase information and share identical stationary point-pairs, therefore we can refer directly to the analysis in the previous section.

We focus on $\mathfrak{A}^{\boldsymbol{A}}[G^S_{x',x_1}; G^S_{x',x}; G^S_{x_2,x}]$ and therefore construct purely causal scattered waves [see Eq. (22)]. In practice, it is not always possible to discriminate between direct and scattered wavefields. However, we assume that at least for one point-pair (x',x), the scattered fields $G^S(x',x_1)$, $G^S(x_2,x)$, and $G^{S*}(x',x)$ can be distinguished from the corresponding direct waves. Such a single pair will be shown to be enough to provide a construction of the scattered-wave Green's function between x_1 and x_2. This is extremely favorable for applications as it removes the need for either source or receiver coverage at prescribed stationary boundary locations (which are not usually predictable in advance if the scatterer position is unknown), as is always required in the inter-receiver case. In addition, it enormously lightens computational burden as only a few Green's function need to be computed or measured. This not only saves CPU time but also memory, since it obviates the need to store the large integrand data arrays that appear to be necessary to compute equation (6).

Figure 6 shows the geometrical configuration of our synthetic tests. In Figs. 7(A) and 7(B), the solid trace shows the true scattered field $G^S(x_2,x_1)+G^{S*}(x_2,x_1)$ while the dashed trace represents the wavefield constructed from evaluation of $\mathfrak{A}^{\boldsymbol{A}}[G^S_{x',x_1}; G^S_{x',x}; G^S_{x_2,x}]$. To calculate the latter field we have used the complete source and receiver boundaries in Fig. 6 as prescribed by Eq. (6), but only one out of the seven terms indicated in Eq. (22), namely, $\mathfrak{A}^{\boldsymbol{A}}[G^S_{x',x_1}; G^S_{x',x}; G^S_{x_2,x}]$. For this reason, only the causal part of the Green's function is recovered by interferometry. To compensate for the missing integrals and to provide a better comparison between the two waveforms, we normalize both signals by their maximum amplitudes. The match between the two traces is excellent. This indicates that only absolute amplitude information would be added by the seven ignored terms: the correct waveform shape is intrinsic to $\mathfrak{A}^{\boldsymbol{A}}[G^S_{x',x_1}; G^S_{x',x}; G^S_{x_2,x}]$, and hence it predicts relative amplitudes of different frequencies correctly for isotropic scatterers [see Eq. (24)].

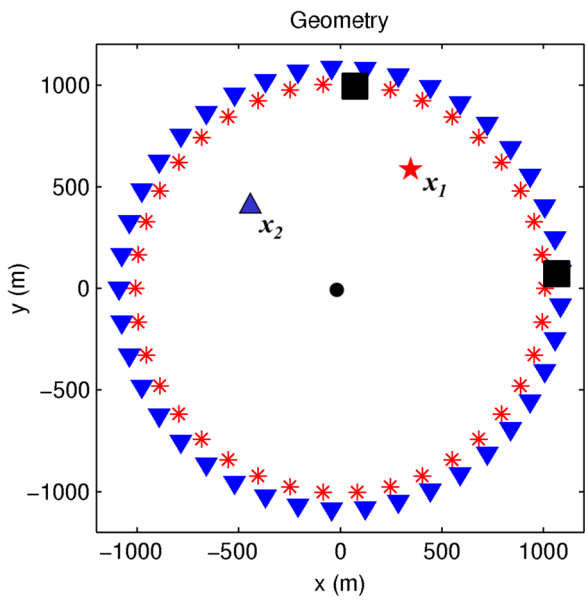

FIG. 6. (Color online) Geometry used for the synthetic example. Asterisks and triangles indicate sources and receivers, respectively. The large squares correspond to the single source-receiver pair used for the "minimal" experiment referred to in the text and in Fig. 7.

We can go one step further and choose to use a minimal information: we approximate the estimate of $\mathfrak{A}^{\boldsymbol{A}}[G^S_{x',x_1}; G^S_{x',x}; G^S_{x_2,x}]$ by the value of its integrand at a single random point pair (x',x) shown in Fig. 6 by squares (which are nowhere near the various stationary point-pairs depicted earlier). This attempt to retrieve the scattered Green's function results in the reconstruction provided in Figs. 7(C) and 7(D). Again, interferometry can only retrieve the causal part of the Green's function, and once more normalization has been applied to account for the limited number of sources employed. Despite the approximations involved, the match remains excellent. This confirms that the correct waveform information is not only intrinsic in $\mathfrak{A}^{\boldsymbol{A}}[G^S_{x',x_1}; G^S_{x',x}; G^S_{x_2,x}]$, but it is also inherent in the function $G^S(x',x_1)G^S(x_2,x)$ $G^{S*}(x',x)$ for any pair $(x',\ x)$ in the case of isotropic point scatterers.

IV. DISCUSSION

The first application to a real seismic data set of SRI (Duguid *et al.*, 2011) indicated its apparently superior ability to construct Green's functions over standard cross-correlational or convolutional inter-receiver interferometric methods. That test is particularly relevant because in that experiment the partial approximation of the theoretical requirements was worse for the source-receiver case than for the inter-receiver experiments (approximately only 1/24 and 1/6 of the theoretically required data were used for source-receiver and inter-receiver interferometry, respectively). While an exhaustive explanation to this improved performance has not been formulated to date, both for reflections (Poliannikov, 2011; King and Curtis, 2012) and refractions (Bharadwaj *et al.*, 2011) this has been discussed in the context of transforming non-physical energy into physical energy. More precisely, it has been shown that the combination of cross-correlation and convolution in SRI shifts non-physical, non-stationary energy in the inter-receiver case into physical, stationary energy in the source-receiver case. We have now shown here that such a conversion takes place for any singly-scattered data.

Curtis *et al.* (2012) showed that SRI faithfully produced real earthquake seismograms even into the coda, at receivers installed only after the earthquake occurred, despite using only a partial receiver boundary which spanned the highest attenuation zone in New Zealand. This was unexpected because the theory used was virtually the same as is examined here, and is theoretically only valid for elastic (lossless) media. However, the fact that a proxy for the scattered energy is contributed by *any* source and receiver may explain the apparent robustness of the method, as sources

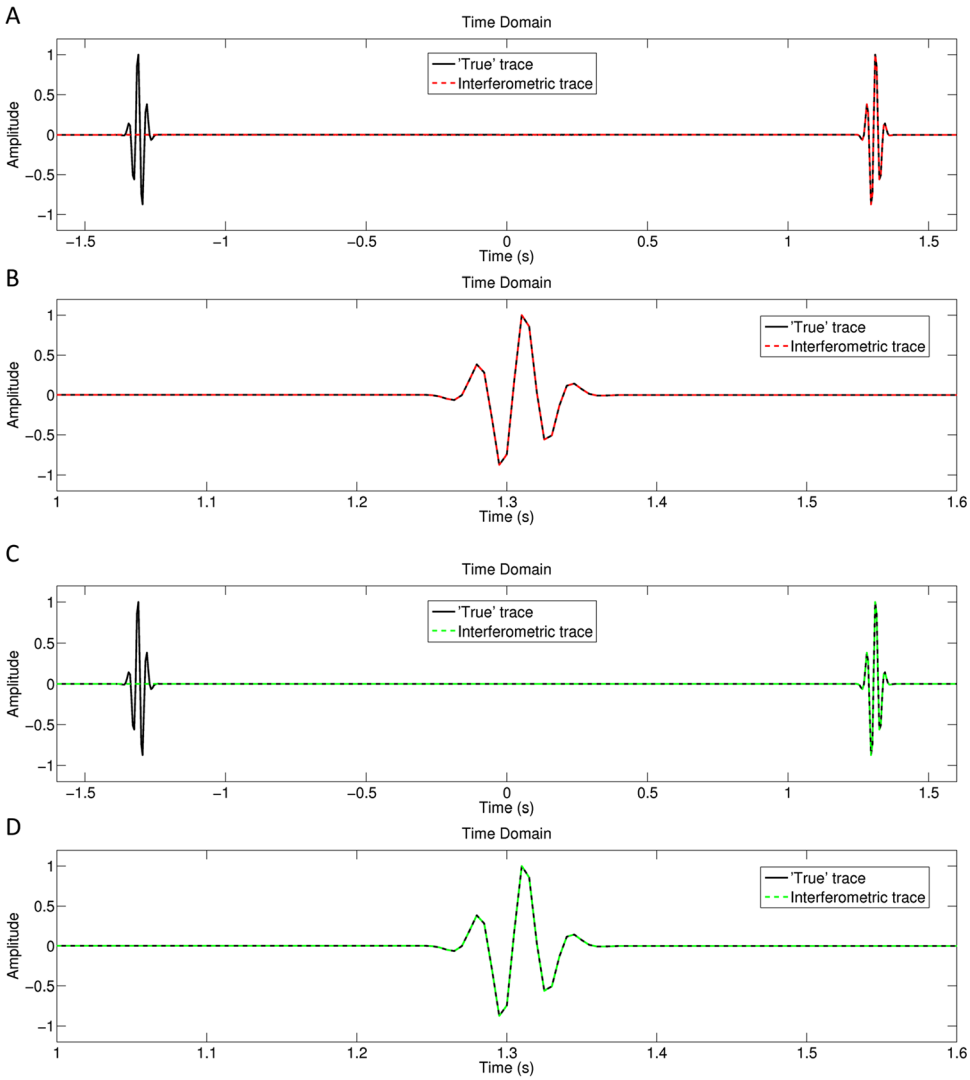

FIG. 7. (Color online) (A) True scattered (solid trace) and interferometrically constructed wavefield (dashed trace), each normalized by its maximum amplitude. To calculate the scattered field the complete source and receiver boundaries in Fig. 6 were used, but only one out of the seven terms indicated in Eq. (22), namely, $\mathfrak{L}^A[G^S_{x',x_1}; G^S_{x',x}; G^S_{x_2,x}]$, was employed. For this reason, only the causal part of the Green's function is recovered by interferometry. (B) As for (A), but zoomed in to show the causal arrival. (C) and (D) are as for (A) and (B), but the minimal configuration, which only involves one source and one receiver (see Fig. 6) was used.

and receivers outside of the high attenuation zone would all have contributed physically scattered energy to the reconstructed coda.

In inter-receiver interferometry, purely scattered waves only produce non-physical energy, for which the completeness of the boundary compensates. In SRI, the intrinsic coherency of each single scattering event can foster the construction of physical singly scattered wavefields for any energy arriving at the scatterer, no matter what the previous scattering and reflecting history of that energy might be. This allows the different scattering events to be considered as being partially decoupled from the complexity of the multi scatterer-reflection scenario, thus improving the quality of constructed Green's functions. The fact that the physical scattered waves can always be constructed from *any* illuminating boundary source and receiver also means that physical scattered waves can in principle be discriminated from non-physical energy, even when boundaries are severely limited in aperture (as is usually in practical problems). This should be useful in future practical applications. While theoretically limited to the simple and ideal case of a single scatterer, similar or related results are valid also for multiple scatterer problems (Meles and Curtis, 2013).

In our numerical examples we have considered an isotropic scatterer, but the validity of the arguments discussed in Sec. II naturally extends also to kinematic analysis of any scatterer. For anisotropic scatterers, however, inaccuracies may be introduced in the Green's function estimates when arbitrary point pairs are used to approximate the scattered field through evaluation of only $\mathfrak{L}^A[G^S_{x',x_1}; G^S_{x',x}; G^S_{x_2,x}]$. A detailed analysis of these topics in source-receiver interferometry may be the subject of future research.

V. CONCLUSIONS

We express the source-receiver interferometric integral as the superposition of eight terms involving different combinations of direct and scattered fields. Then we deduce a new representation for the scattered wavefield in source-receiver interferometry, involving only surface integrals. The new expression for the scattered field leads naturally to a systematic analysis of stationary points, and allows us to explain why for the single scatterer problem, source-receiver interferometry has been observed to be more stable than inter-receiver interferometry when constructing scattered wave information: any and every pair of a source and a receiver anywhere in the medium is sufficient to produce an excellent

proxy for the correct physical contribution to the scattered wavefield between any other source and receiver pair. This avoids ambiguity in the Green's functions construction, and can be used to discriminate between correct and spurious events. The same result can hold when energy arriving at the scatterer is multiply scattered by other diffractors or reflectors, as will often be the case in real-world situations.

ACKNOWLEDGMENTS

The authors are grateful to Ivan Vasconcelos (Schlumberger Gould Research, UK) for insightful discussions. We also thank the Edinburgh Interferometry Project (EIP) sponsors (ConocoPhillips, Schlumberger, Statoil, and Total) for supporting this research.

Bakulin, A., and Calvert, R. (**2004**). "Virtual source: New method for imaging and 4D below complex overburden," *74th Annual International Meeting, SEG*, Expanded Abstracts, pp. 2477–2480.

Bakulin, A., and Calvert, R. (**2006**). "The virtual source method: Theory and case study," Geophysics **71**(4), SI139–SI150.

Bharadwaj, P., Schuster, G., Mallinson, I., and Dai, W. (**2011**). "Theory of supervirtual refraction interferometry," Geophys. J. Int. **178**, 419–446.

Campillo, M., Paul, A. (**2003**). "Long range correlations in the seismic coda," Science **299**, 547–549.

Claerbout, J. F. (**1968**), "Synthesis of a layered medium from its acoustic transmission response," Geophysics **33**, 264–269.

Curtis, A., Behr, Y., Entwistle, E., Galetti, E., Townend, J., and Bannister, S. (**2012**). "The benefit of hindsight in observational science: retrospective seismological observations," Earth Planet. Sci. Lett. **345–348**, 212–220.

Curtis, A., Gerstoft, P., Sato, H., Snieder, R., and Wapenaar, K. (**2006**). "Seismic interferometry—Turning noise into signal," The Leading Edge **25**, 1082–1092.

Curtis, A., and Halliday, D. (**2010**). "Source-receiver wave field interferometry," Phys. Rev. E **81**, 046601.

Curtis, A., Nicolson, H., Halliday, D., Trampert, J., and Baptie, B. (**2009**). "Virtual seismometers in the subsurface of the Earth from seismic interferometry," Nat. Geosci. **2**, 700–704.

Derode, A., Larose, E., Campillo, M., and Fink, M. (**2003**). "How to estimate the Green's function of a heterogeneous medium between two passive sensors? Application to acoustic waves," Appl. Phys. Lett. **83**, 3054–3056.

Dong, S., He, R., and Schuster, G. (**2006**). "Interferometric prediction and least square subtraction of surface waves," *76th Annual International Meeting, SEG*, Expanded Abstracts, pp. 2783–2786.

Duguid, C., Halliday, D., and Curtis, A. (**2011**). "Source-receiver interferometry for seismic wavefield construction and ground roll removal," The Leading Edge **30**, 838–843.

Fleury, C., Snieder, R., and Larner, K. (**2010**). "General representation theorem for perturbed media and application to Green's function retrieval for scattering problems," Geophys. J. Int. **183**, 1648–1662.

Fleury, C., and Vasconcelos, I. (**2012**). "Imaging condition for nonlinear scattering-based imaging: Estimate of power loss in scattering," Geophysics **77**, S1–S18.

Foldy, L. L. (**1945**). "The multiple scattering of waves. I. General theory of isotropic scattering by randomly distributed scatterers," Phys. Rev. **67**, 107–119.

Galetti, E., and Curtis, A. (**2012**). "Generalised receiver functions and seismic interferometry," Tectonophysics **6**, 1–26.

Galetti, E., Halliday, A., and Curtis, A. (**2013**). "A simple and exact acoustic wavefield modelling code for data processing, imaging and interferometry applications," Geophysics (in press).

Groeneboom, J., and Snieder, R. (**1995**). "Attenuation, dispersion, and anisotropy by multiple scattering of transmitted waves through distributions of scatterers," J. Acoust. Soc. Am. **98**, 3482–3492.

Halliday, D., and Curtis, A. (**2009**). "Generalized optical theorem for surface waves and layered media," Phys. Rev. E **79**, 056603.

Halliday, D., and Curtis, A. (**2010**). "An interferometric theory of source-receiver scattering and imaging," Geophysics **75**, SA95–SA103.

Halliday, D., Curtis, A., Robertsson, J. O. A., and van Manen, D. J. (**2007**). "Interferometric surface-wave isolation and removal," Geophysics **72**, A69–A73.

Halliday, D., Curtis, A., Vermeer, P., Strobbia, C., Glushchenko, A., van Manen, D. J., and Robertsson, J. O. A. (**2010**). "Interferometric ground-roll removal: Attenuation of direct and scattered surface waves in single-sensor data," Geophysics **75**, SA15–SA25.

Hong, T. K., and Menke, W. (**2006**). "Tomographic investigation of the wear along the San Jacinto fault, southern California," Phys. Earth Planet. Int. **155**, 236–248.

King, S., and Curtis, A. (**2011**). "Velocity analysis using both reflections and refractions in seismic interferometry," Geophysics **76**, SA83–SA96.

King, S., and Curtis, A. (**2012**). "Suppressing nonphysical reflections in Green's function estimates using source-receiver interferometry," Geophysics **77**, Q15–Q25.

King, S., Curtis, A., and Poole, T. (**2011**). "Interferometric velocity analysis using physical and nonphysical energy," Geophysics **76**(1), SA35–SA49.

Meles, G. A., and Curtis, A. (**2013**). "Discriminating Physical and Non-Physical Energy in Wavefield Interferometry," *75th EAGE Conference*, EAGE Expanded Abstract.

Mikesell, D., van Wijk, K., Calvert, A., and Haney, M. (**2009**). "The virtual refraction: Useful spurious energy in seismic interferometry," Geophysics **74**, A13–A17.

Poliannikov, O. V. (**2011**). "Retrieving reflections by source-receiver wavefield interferometry," Geophysics **76**, SA1–SA8.

Poliannikov, O. V., Rondenay, S., and Chen, L. (**2012**). "Interferometric imaging of the underside of a subducting crust," Geophys. J. Int. **189**(1), 681–690.

Ravasi, M., and Curtis, A. (**2013**). "Nonlinear scattering based imaging in elastic media: Theory, theorems and imaging conditions," Geophysics **78**(3), S137–S155, doi:10.1190/GEO2012-0286.1.

Rickett, J., and Claerbout, J. (**1999**). "Acoustic daylight imaging via spectral factorization: Helioseismology and reservoir monitoring," The Leading Edge **18**, 957–960.

Sava, P., and Vasconcelos, I. (**2010**). "Extended imaging condition for wave-equation migration," Geophys. Prospec. **59**, 35–55.

Schuster, G., and Rickett, J. (2000). "Daylight imaging in V(x,y,z) media, Utah Tomography and Modeling-Migration Project," Midyear Report and SEP Report at Stanford University.

Schuster, G., Sheng, J. Yu and Rickett J. (**2004**). "Interferometric/daylight seismic imaging," Geophys. J. Int. **157**, 838–852.

Schuster, G., and Zhou, M. (**2006**). "A theoretical overview of model-based and correlation-based redatuming methods," Geophysics **71**, SI103–SI110.

Schuster, G. T. (**2009**). *Seismic Interferometry* (Cambridge University Press, Cambridge), pp. 1–260.

Slob, E., Draganov, D., and Wapenaar, K. (**2007**). "Interferometric electromagnetic Green's functions representations using propagation invariants," Geophys. J. Int. **169**, 60–80.

Snieder, R. (**2004**). "Extracting the Green's function from the correlation of coda waves: A derivation based on stationary phase," Phys. Rev. E **69**, 046610.

Snieder, R., and Fleury, C. (**2010**). "Cancellation of spurious arrivals in Green's function retrieval of multiple scattered waves," J. Acoust. Soc. Am. **128**, 1598–1605.

Snieder, R., van Wijk, K., Haney, M., and Calvert, R. (**2008**). "Cancellation of spurious arrivals in Green's function extraction and the generalized optical theorem," Phys. Rev. E. **78**, 036606.

Snieder, R., Wapenaar, K., and Larner, K. (**2006**). "Spurious multiples in seismic interferometry of primaries," Geophysics **78**, SI111–SI124.

Thorbecke, J., and Wapenaar, K. (**2007**). "On the relation between seismic interferometry and the migration resolution function," Geophysics **72**, T61–T66.

van Manen, D. J., Curtis, A., and Robertsson, J. O. A. (**2006**). "Interferometric modeling of wave propagation in inhomogeneous elastic media using time reversal and reciprocity," Geophysics **71**, SI47–SI60.

van Manen, D. J., Robertsson, J. O. A., and Curtis, A. (**2005**). "Modeling of wave propagation in inhomogeneous media," Phys. Rev. Lett. **94**(16), 164301.

Vasconcelos, I. (**2011**). "Source-receiver reverse-time imaging of vector-acoustic seismic data," *81st Annual International Meeting*, SEG Expanded Abstracts, pp. 3184–3189.

Vasconcelos, I., Sava, P., and Douma, H. (**2010**). "Nonlinear extended images via image-domain interferometry," Geophysics **75**, SA105–SA115.

Vasconcelos, I., Snieder, R., and Douma, H. (**2009**). "Representation theorems and Green's function retrieval for scattering in acoustic media," Phys. Rev. E **80**, 036605.
Wapenaar, K. (**2003**), "Synthesis of an inhomogeneous medium from its acoustic transmission response," Geophysics **68**, 1756–1759.
Wapenaar, K. (**2004**), "Retrieving the elastodynamic Green's function of an arbitrary inhomogeneous medium by cross correlation," Phys. Rev. Lett. **93**, 254301.
Wapenaar, K., Draganov, D., Snieder, R., Campman, X., and Verdel, A. (**2010a**). "Tutorial on seismic interferometry: Part 1—Basic principles and applications," Geophysics **75**, A195–A209.
Wapenaar, K., and Fokkema, J. (**2006**). "Green's function representations for seismic interferometry," Geophysics **71**, SI33–SI46.
Wapenaar, K., Slob, E., and Snieder, R. (**2010b**). "On seismic interferometry, the generalized optical theorem and the scattering matrix of a point scatterer," Geophysics **75**, SA27–SA35.
Wapenaar, K., Slob, E., Snieder, R., and Curtis A. (**2010c**). "Tutorial on seismic interferometry: Part 2—Underlying theory and new advances," Geophysics **75**, A211–A227.
Xue, Y., and Schuster, G. (**2007**). "Surface-wave elimination by interferometry with nonlinear local filter," *77th Annual International Meeting*, SEG Expanded Abstracts, pp. 2620–2624.